

# Broadband photonic ADC for microwave photonics-based radar receiver

Jiaqian Yang (杨佳骞), Shangyuan Li (李尚远), Xuedi Xiao (肖雪迪), Dexin Wu (吴德鑫), Xiaoxiao Xue (薛晓晓), and Xiaoping Zheng (郑小平)\*

*Tsinghua National Laboratory for Information Science and Technology, Department of Electronic Engineering, Tsinghua University, Beijing 100084, China*

\*Corresponding author: xpzheng@mail.tsinghua.edu.cn

Received February 9, 2018; accepted April 19, 2018; posted online May 28, 2018

A broadband photonic analog-to-digital converter (ADC) for X-band radar applications is proposed and experimentally demonstrated. An X-band signal with arbitrary waveform and a bandwidth up to 2 GHz can be synchronously sampled and processed due to the optical sampling structure. In the experiment, the chirp signal centered at 9 GHz with a bandwidth of 1.6 GHz is sampled and down-converted with a signal-to-noise ratio of 7.20 dB and an improved noise figure. Adopting the photonic ADC in the radar receiver and the above signal as the transmitted radar signal, an X-band inverse synthetic aperture radar system is set up, and the range and cross-range resolutions of 9.4 and 8.3 cm are obtained, respectively.

OCIS codes: 060.5625, 320.5520.

doi: 10.3788/COL201816.060605.

Radar has been used in target detection, tracking, and imaging for a long time. Broad signal bandwidth can result in higher resolution, and low noise in data conversion leads to high precision. Recent electronic radar systems are facing the above challenges as the carrier frequency increases. However, photonics can provide ultrastable optical pulses and ultrawide bandwidth, thus, radar systems can benefit a lot from the development of microwave photonic technology<sup>[1–3]</sup>. An architecture of the photonics-based radar was proposed consisting of a photonics-based RF generator, a photonics-based analog-to-digital converter (ADC), and a digital signal processor<sup>[4]</sup>. Limited by the performance of mode-locked lasers (MLLs), the system achieved a 400 MHz sampling rate, so the bandwidth of the signal being processed could be extended up to 200 MHz, which may hardly meet the requirement of current radar systems. To handle this problem, several microwave photonics-based radar systems have been established, focusing on frequency doubling<sup>[5]</sup>, optical arbitrary waveform generation (OAWG)<sup>[6]</sup>, inverse synthetic aperture radar (ISAR) imaging, and de-chirp algorithms in radar receivers. As the de-chirp method in radar receiver reduces the sampling rate dramatically, real-time imaging could be achieved<sup>[7–9]</sup>. However, such a method is only valid for linear frequency modulated (LFM) signals. What is more, in long distance ranging, this technique will cause a signal-to-noise ratio (SNR) loss due to time delay<sup>[10]</sup>. As photonic ADC adopts an optical sampling scheme, it can be used in an undersampling mode for frequency down-conversion, and this kind of frequency conversion is synchronous with sampling pulses and electronic ADC, so stable phases could be acquired in the sampled data. Therefore, photonic ADC-based radar receivers have great potential in improving noise figure and implementing precise data conversion. The waveform of the

signal is no longer limited, and the bandwidth could be extended to several gigahertz.

Traditional electronic ADCs can no longer meet the need of current applications, such as radar receivers, space and defense applications, and software defined radio<sup>[11–13]</sup>. The accuracy of conversion, mainly affected by aperture jitter, has been boosted since the proposal of photonic ADC<sup>[14,15]</sup>. With great advantages of microwave photonics, such as ultrastable optical pulses, large bandwidths capable of being processed, and anti-interference ability<sup>[16–18]</sup>, photonic ADCs have reached high sampling rate and high SNR at the same time. Time-wavelength interleaved photonic ADC has reached 9.0 effective number of bits (ENOB) for 0.2 GHz input and 6.4 bits for 6.1 GHz input with a sampling rate of 20 GSa/s, due to the third harmonic suppression by dual-output modulation<sup>[19]</sup>. With multi-channel mismatches compensation, the performance further boosts to 8.5 bits for 0.1–3.1 GHz input and 7.5 bits for 3.1–12.1 GHz input with 40 GSa/s sampling<sup>[20]</sup>. However, seldom have researchers used photonic ADC in broadband radar receivers because the frequency response is hardly flat over the whole frequency band, and the delay for signals of different frequencies is not uniform. What is more, the unstable phase between frequency-converted data is an obstacle on radar ranging and imaging. Thus, we use the system function to establish a photonic ADC system with uniform frequency response and delay performance over 8 to 10 GHz frequency band, and synchronization between the radar signal and sampling pulses ensures stable phases and low noise. The pulse compressing algorithm for ranging and imaging also brings about the sharp increase in SNR, which makes photonic ADC a suitable system in broadband radar receivers.

In this Letter, a broadband photonic ADC for X-band radar applications with flat frequency response over the

8 to 10 GHz frequency band is proposed and experimentally tested in a radar system. By generation of picosecond optical pulses together with chirp compensation and signal processing, the broadband LFM signal is precisely sampled and down-converted with improved noise figure. In fact, the broadband signal in arbitrary waveform, whose frequency lies in 8 to 10 GHz, could be processed in the proposed radar receiver. By further setting up the ISAR system and detecting the echoed waveform from rotating objects, the range-Doppler map is generated with high range and cross-range resolutions.

The schematic experimental setup of the photonic ADC is shown in Fig. 1.

A high repetition rate optical pulse train is generated by the optical frequency combs and injected into the Mach-Zehnder modulator (MZM), which is driven by the RF signal to be sampled. The modulated optical signal is then converted to the electrical domain by a photodetector (PD), and the down-converted signals can be obtained. Lastly, the electrical signals are digitized by the electronic ADCs. It should be noted that the repetition rate of the pulse train should be greater than two times the bandwidth of the RF signal to avoid spectrum aliasing after sampling.

To demonstrate the evolution of the signal in modulation and optical to electrical conversion, an analysis based on a broadband LFM signal in both time domain and frequency domain is undertaken. We assume that the input LFM signal is

$$V_{\text{in}}(t) = V_s \cos \left[ 2\pi \left( f_0 t + \frac{1}{2} \frac{B}{T} t^2 \right) \right], \quad (1)$$

where  $f_0$  is the start frequency of the signal,  $B$  is the bandwidth,  $T$  is the pulse width, and  $V_s$  is its amplitude. The input signal is then fed into the MZM operated at the quadrature point. The optical field at the output of the MZM can be written as

$$E_{\text{MZM}}(t) = E_{\text{in}}(t) \cos \left\{ \frac{\pi}{2V_\pi} [V_{\text{in}}(t) + V_b] \right\} e^{j\varphi_M}, \quad (2)$$

where  $E_{\text{in}}$  represents the input optical pulse train,  $V_\pi$  is the half-wave voltage of the MZM,  $V_b$  is direct-current (DC) bias voltage and is set to be  $V_\pi/2$ , so that

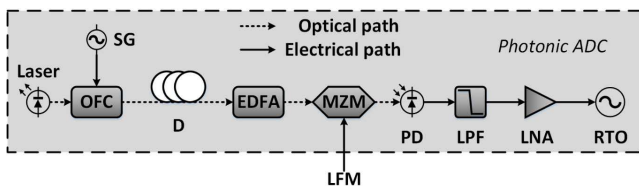


Fig. 1. Schematic of the photonic ADC. OFC, optical frequency comb; SG, signal generator; D, dispersion; EDFA, erbium-doped fiber amplifier; MZM, Mach-Zehnder modulator; PD, photodetector; LPF, low pass filter; LNA, low noise amplifier; RTO, real-time oscilloscope.

$\cos 2\varphi_b = 0$ , and  $\sin 2\varphi_b = 1$ .  $\varphi_M$  is the phase shift induced by the MZM. By substituting Eq. (1) into Eq. (2) and using the Jacobi-Anger expansion, we calculate the photocurrent after photo-detection using the formula  $I(t) = \Re |E_{\text{MZM}}(t)|^2$ , where  $\Re$  represents the responsivity of the PD:

$$I(t) = \frac{1}{2} \Re |E_{\text{in}}|^2 \left\{ \begin{array}{l} 1 - 2J_1(2m) \cos 2\pi \left( f_0 t + \frac{1}{2} \frac{B}{T} t^2 \right) + \\ 2J_3(2m) \cos 6\pi \left( f_0 t + \frac{1}{2} \frac{B}{T} t^2 \right) + \dots \end{array} \right\}, \quad (3)$$

where  $m = \pi V_s / 2V_\pi$  represents the modulation index of the MZM.

Here, we neglect terms for  $n \geq 5$  as  $J_n(2m)$  is negligible compared with the first two terms. In Eq. (3), the  $2J_1(2m)$  term is the original LFM signal, and the  $2J_3(2m)$  term is the third-order harmonic distortion that can be controlled to a low level by delicately controlling the LFM signal power, in other words, the modulation index  $m$ .  $|E_{\text{in}}|^2$  is the optical input, which corresponds to the envelope of the input optical pulse train to sample or frequency down-convert the LFM signal.

When sampling broadband signals, the spectrum of the signal experiences a periodical extension after photodetection, and one can obtain the frequency down-converted signal using a low pass filter (LPF) with a certain bandwidth and a DC block. The bandwidth of the sampled signal can be obtained by subtracting multiples of the sampling rate from the original signal bandwidth, which means the slew rate of the signal dropped dramatically. Therefore, the amplitude noise induced by aperture jitter will be reduced. Thus, it lowers the requirement of subsequent electronic ADCs.

In the experiment, an optical frequency comb centered at 1552.25 nm with 4 GHz spacing is generated by cascading an intensity modulator and a phase modulator<sup>[2]</sup>. A  $-100$  ps/nm dispersion compensation fiber and an erbium-doped fiber amplifier (EDFA) are used to further compress and amplify the optical signal, generating an optical pulse train with 4 GHz repetition rate and about 10 ps pulse width. An X-band LFM signal centered at 9 GHz with a bandwidth of 1.6 GHz modulates the pulse train at the MZM (Photline, MX-LN-10). The LFM signal is frequency synchronized with optical pulses to ensure precise sampling points. Then, the modulated pulse train is detected at the PD (u2 t, XPDV2120RA), and the electrical signal is further filtered by a 2 GHz bandwidth LPF and amplified by a low noise amplifier (LNA). A real-time oscilloscope (ROHDE&SCHWARZ, RTO 1022) is used instead of electronic ADCs to digitize the sampled signal before digital signal processing.

The waveforms before and after photonic ADC sampling are shown in Fig. 2. The broadband LFM signal with a bandwidth of 1.6 GHz is precisely sampled and down-converted to 0.2 to 1.8 GHz. Over the whole frequency band, the flatness of the proposed ADC is measured to

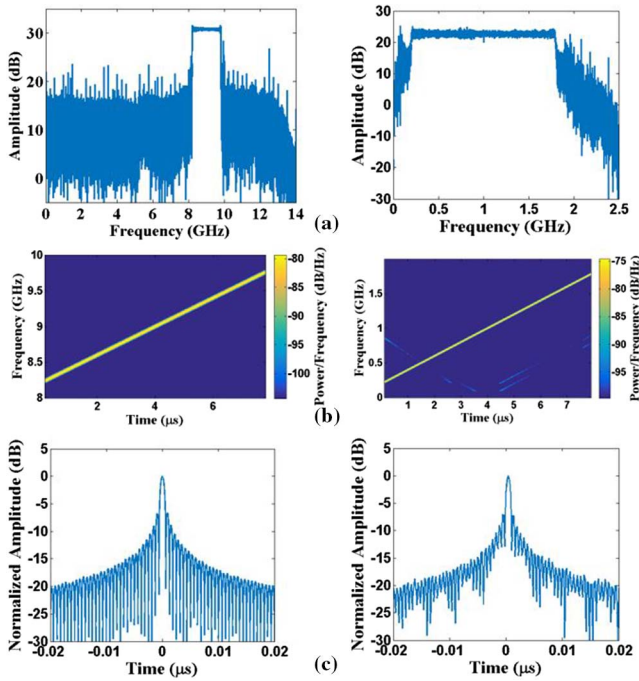


Fig. 2. Results before and after photonic ADC sampling. (a) Spectrum. (b) Short-time Fourier transform (STFT) analysis. (c) Results after pulse compression.

be 5.18 dB, compared with the original X-band signal with a flatness of 1.71 dB. There are some image frequency components due to the nonlinearity of the oscilloscope, and they could be further eliminated using digital signal processing. Nevertheless, they have little effect on radar ranging and imaging. The symmetry of the pulse compression result with an error of less than 0.2 dB shows that the delay in optical and electrical paths is calibrated. Therefore, the proposed photonic ADC with flat frequency response and uniform delay performance is capable of receiving X-band radar signals.

In radar receivers, the noise figure is the deterioration of SNR from the input of the receiver to the output. In the proposed system, the degradation of the SNR is mainly attributed to amplitude noise and jitter of the optical pulses, amplified spontaneous emission (ASE) noise of the EDFA, the signal-spontaneous beat noise, and quantization noise, which can be expressed by Eq. (4):

$$\text{SNR} = -10 \log \left[ \delta_A^2 + (2\pi f \sigma_j)^2 + \delta_{\text{EDFA}}^2 + \delta_b^2 + \frac{1}{3 \times 2^{2N-1}} \right]. \quad (4)$$

In our scheme, the primary noise is the timing jitter and ASE noise, which brings a noise figure of 5.4 dB. The main distortion source is the third-order distortion in MZM, but it could be digitally compensated by using the arcsin function<sup>[22]</sup>. The detected signal in Eq. (3) has an amplitude of  $\Re|E_{\text{in}}|^2 J_1(2m)$ . In comparison, the widely used photonic mixer based on the dual-parallel MZM (DPMZM) configuration<sup>[23]</sup> can down-convert an RF signal with an

amplitude of  $2\Re|E_{\text{in}}|^2 J_1(2m_{\text{LO}})J_1(2m_{\text{RF}})$ . The Bessel function is about 0.5 in most cases, so the conversion efficiency is almost the same for the two schemes. However, the proposed sampling method enables the signal to beat with the optical frequency comb at each frequency and sum them up to obtain the final result. During this process, the random beat noise can be eliminated to some extent, rather than only one pair of signals beating with each other in the DPMZM scheme. The synchronous sampling also ensures a stable phase between the sampled data. Therefore, an improved noise figure could be attained. The experiment result shows that the X-band signal is down-converted with a measured SNR of 7.20 dB. The original generated signal has an SNR of 18.53 dB, which means a noise figure of 11.33 dB is obtained. In Ref. [23], a single tone RF signal is down-converted to 80 MHz with a noise figure of 23.5 dB. We also test the noise figure for single tone signals, as shown in Fig. 3. The proposed ADC down-converts a single tone signal from 4.08 GHz to 80 MHz, where the signal power is 2.71 and  $-33.2$  dBm, respectively, and the noise is  $-127$  and  $-151.5$  dBm/Hz, respectively. So, the noise figure is measured to be 11.4 dB. For X-band single tone signals, a noise figure of 12.25–15.84 dB is acquired, which corresponds to the former result for the LFM signal. It can be seen that our proposed photonic ADC shows a better performance in noise figure even if the broadband signal is adopted.

To further test its performance in the radar system, we set up a broadband microwave photonic ISAR platform. Figure 4 shows the schematic of the system based on photonic ADC.

At the transmitter, an electronic arbitrary waveform generator (Tektronix, AWG70002 A) is used to generate a broadband LFM signal centered at 9 GHz with 1.6 GHz bandwidth, 8  $\mu\text{s}$  pulse width, and 100 kHz pulse repetition frequency (PRF). The signal is then amplified by an X-band LNA and transmitted through an antenna. At the receiver, the echoed wave from the targets, namely the rotating platform, is collected by the receiving antenna and amplified before being fed into the MZM in photonic ADC, as shown in Fig. 1.

To test the range resolution of the radar system, two static targets are first located at the center of the rotating platform. After pulse compressing of the echoed wave, the range resolution of about 13 cm is obtained, as shown in

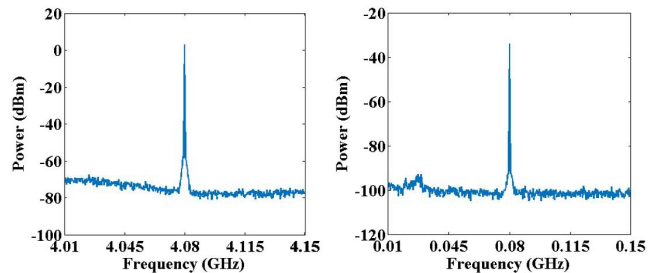


Fig. 3. Spectrum of down-converting a signal from 4.08 GHz to 80 MHz. The measured noise figure is 11.4 dB.

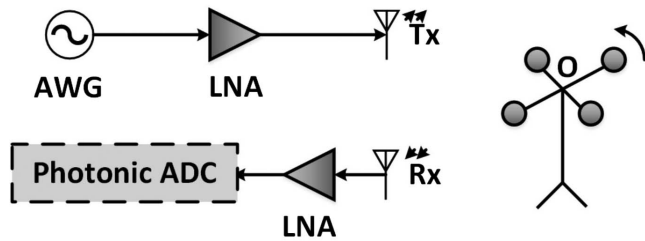


Fig. 4. Schematic of the experimental setup of the broadband microwave photonic ISAR system. AWG, arbitrary waveform generator; LNA, low noise amplifier.

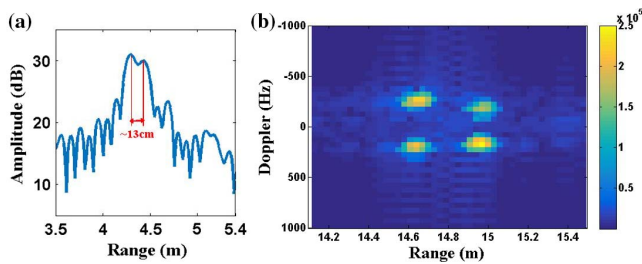


Fig. 5. Results after pulse compression. (a) Pulse compression result of the echoed wave from two static targets. (b) Range-Doppler map of four rotating small balls.

Fig. 5(a), and it still has potential to reach its theoretical value of 9.38 cm.

In the experiment of the rotation imaging system, four 8 cm diameter metal balls rotate counterclockwise around the point  $O$  with a rotation radius of 25 cm. The angular velocity is about 3.5 rounds per second (corresponding to 5.5 m/s linear velocity). Then, 1000 consequent echoed pulses are sampled by a 4 GHz pulse train and accumulated during 10 ms period using the real-time oscilloscope. The range-Doppler imaging algorithm is adopted together with the range tracking and translation compensation. Figure 5(b) shows the range-Doppler map of the echoed wave with a range resolution of  $\sim 10$  cm. The theoretical Doppler and cross-range resolution are 100 Hz and 8.32 cm, respectively.

To further increase the range resolution, a time-interleaved photonic ADC scheme<sup>[14]</sup> could be adopted to increase the sampling rate and bandwidth of the photonic ADC. More echoed pulses could be sampled to prolong the coherent integration time and improve cross-range resolution.

In conclusion, a broadband photonic ADC for X-band radar applications with a theoretical bandwidth of 2 GHz is proposed and experimentally applied in the radar receiver. Broadband radar signals in arbitrary waveform could be processed based on the platform. The high stability and broad bandwidth could be further achieved if OAWG technology is adopted in the transmitter. The experimental results show that the SNR of the broadband photonic ADC is 7.20 dB, and the noise figure of the receiver is around 11.3 dB. Due to the optical sampling

principle, the noise performance is intrinsically better. Further making use of differential detection and real-time digital post-processing would improve system precision by eliminating image frequency components and minimizing spurious tones. Synchronous sampling ensures the stability of the phase in sampled data and precise range detection in radar systems. The experiment result of its application in the ISAR system shows a high range and cross-range resolution of 9.4 and 8.3 cm, respectively, which provides evidence for the application of the proposed photonic ADC in X-band radar receivers.

This work was supported in part by the National Natural Science Foundation of China (NSFC) (Nos. 61690191, 61690192, 61420106003, and 61621064), Chuanxin Funding, and Beijing Natural Science Foundation (No. 4172027).

## References

1. L. Francesco, F. Scotti, P. Ghelfi, A. Bogoni, and S. Pinna, in *2013 IEEE Radar Conference (RADAR)* (2013).
2. L. Pierno, M. Dispenza, G. Tonelli, A. Bogoni, P. Ghelfi, and L. Poti, in *2008 IEEE International Meeting on Microwave Photonics Jointly Held with the 2008 Asia-Pacific Microwave Photonics Conference, MWP2008/APMP2008* (2008), p. 236.
3. F. Laghezza, F. Scotti, P. Ghelfi, and A. Bogoni, *J. Lightwave Technol.* **32**, 2896 (2014).
4. P. Ghelfi, F. Laghezza, F. Scotti, G. Serafino, A. Capria, S. Pinna, D. Onori, C. Porzi, M. Scaffardi, A. Malacarne, V. Vercesi, E. Lazzeri, F. Berizzi, and A. Bogoni, *Nature* **507**, 341 (2014).
5. R. Li, W. Li, M. Ding, Z. Wen, Y. Li, L. Zhou, S. Yu, T. Xing, B. Gao, Y. Luan, Y. Zhu, P. Guo, Y. Tian, and X. Liang, *Opt. Express* **25**, 14334 (2017).
6. X. Xiao, S. Li, B. Chen, X. Yang, D. Wu, X. Xue, X. Zheng, and B. Zhou, in *CLEO: Science and Innovations* (2017), paper JW2A-144.
7. F. Zhang, Q. Guo, Z. Wang, P. Zhou, G. Zhang, J. Sun, and S. Pan, *Opt. Express*, **25**, 16274 (2017).
8. F. Zhang, Q. Guo, and S. Pan, *Sci. Rep.* **7**, 13848 (2017).
9. F. Zhang, Q. Guo, Y. Zhang, Y. Yao, P. Zhou, D. Zhu, and S. Pan, *Chin. Opt. Lett.* **15**, 112801 (2017).
10. T. Long, Y. Wang, and T. Zeng, *Electron. Lett.* **46**, 720 (2010).
11. R. H. Walden, ed., *Wiley Encyclopedia of Computer Science and Engineering* (Wiley, 2008).
12. M. A. Piqueras, P. Villalba, J. Puche, and J. Marti, in *2011 IEEE International Conference on Microwaves, Communications, Antennas and Electronics Systems (COMCAS)* (2011) p. 1.
13. R. H. Walden, in *IEEE J. Sel. Areas Commun.* **17**, 539 (1999).
14. A. Khilo, S. J. Spector, M. E. Grein, A. H. Nejadmalayeri, C. W. Holzwarth, M. Y. Sander, M. S. Dahlem, M. Y. Peng, M. W. Geis, N. A. DiLello, J. U. Yoon, A. Motamedi, J. S. Orcutt, J. P. Wang, C. M. Sorace-Agaskar, M. A. Popović, J. Sun, G.-R. Zhou, H. Byun, J. Chen, J. L. Hoyt, H. I. Smith, R. J. Ram, M. Perrott, T. M. Lyszczarz, E. P. Ippen, and F. X. Kärtner, *Opt. Express* **20**, 4454 (2012).
15. J. E. Daniel, A. O. J. Wiberg, N. Alic, and S. Radic, *J. Lightwave Technol.* **33**, 2256 (2015).
16. J. Capmany and D. Novak, *Nat. Photon.* **1**, 319 (2007).
17. J. Yao, *J. Lightwave Technol.* **27**, 314 (2009).
18. R. A. Minasian, *IEEE Trans. Microwave Theory Tech.* **54**, 832 (2006).
19. H. Zhang, W. Zou, G. Yang, and J. Chen, *Chin. Opt. Lett.* **14**, 030602 (2016).

20. G. Yang, W. Zou, L. Yu, K. Wu, and J. Chen, *Opt. Express* **24**, 24061 (2016).
21. R. Wu, V. R. Supradeepa, C. M. Long, D. E. Leaird, and A. M. Weiner, *Opt. Lett.* **35**, 3234 (2010).
22. T. R. Clark, M. Currie, and P. J. Matthews, *J. Lightwave Technol.* **19**, 172 (2001).
23. H. W. Erwin, *J. Lightwave Technol.* **30**, 3580 (2012).